PPS
Paper
www.rsc.org/pps

Ruthenium(II)–tris-bipyridine/titanium dioxide codoped zeolite Y photocatalysts: II. Photocatalyzed degradation of the model pollutant 2,4-xylidine, evidence for percolation behavior †

Stefan H. Bossmann,*[a] Steffen Jockusch,[b] Peter Schwarz,[b] Bodo Baumeister,[a] Sabine Göb,[a] Claudia Schnabel,[a] Leon Payawan, Jr.,[a] Megh Raj Pokhrel,[a] Michael Wörner,[a] André M. Braun *[a] and Nicholas J. Turro *[b]

[a] *Lehrstuhl für Umweltmesstechnik am Engler-Bunte-Institut der Universität Karlsruhe, 76128 Karlsruhe, Germany. E-mail: Stefan.Bossmann©ciw.uni-karlsruhe.de; Andre.Braun©ciw.uni-karlsruhe.de*

[b] *Department of Chemistry, Columbia University, New York, NY 10027, USA. E-mail: turro@chem.columbia.edu*

Received 16th December 2002, Accepted 13th March 2003
First published as an Advance Article on the web 4th April 2003

A considerably arduous test of a novel class of composite materials consisting of $[Ru(bpy)_3]^{2+}$ and TiO_2 codoped zeolites Y is presented here. The $[Ru(bpy)_3]^{2+}$ and TiO_2 codoped zeolites Y served as photocatalysts in the oxidation of the model compounds 2,4-dimethylaniline (2,4-xylidine) by H_2O_2 in an acidic aqueous medium. Zeolite-embedded TiO_2 (nano)particles play an important role in the degradation mechanism. The first step in this complex mechanism is the photoelectron transfer from photoexcited $[Ru(bpy)_3]^{2+}$*, located inside the supercage of zeolite Y, to a neighboring TiO_2 nanoparticle. During this electron transfer process, electron injection into the conduction band of TiO_2 is achieved. The second decisive step is the reaction of this electron with H_2O_2, which was previously chemisorbed at the surface-region of the TiO_2 nanoparticles. In this reaction, a TiO_2 bound hydroxyl radical (TiO_2–$HO^{\bullet}$) is created. This highly reactive intermediate initiates then the oxidation of 2,4-xylidine, which enters the zeolites framework in its protonated form ($Hxyl^+$). The formation of 2,4-dimethylphenol as first detectable reaction product indicated that this oxidation proceeds *via* an electron transfer mechanism. Furthermore, $[Ru(bpy)_3]^{3+}$, which was created in the initiating photoelectron transfer reaction between $[Ru(bpy)_3]^{2+}$* and TiO_2, also takes place in the oxidation of $Hxyl^+$. $[Ru(bpy)_3]^{2+}$ is recycled in that reaction, which also belongs to the group of electron transfer reactions. In addition to the primary steps of this particular Advanced Oxidation Process (AOP), the dependence of the efficiency of the 2,4-xylidine degradation as a function of the $[Ru(bpy)_3]^{2+}$ and TiO_2 loadings of the zeolite Y framework is also reported here. The quenching of $[Ru(bpy)_3]^{2+}$* by H_2O_2 as well as the photocatalytic activity of the $[Ru(bpy)_3]^{2+}$ and TiO_2 codoped zeolite Y catalysts both follow a distinct percolation behavior in dependence of their TiO_2 content.

Introduction

In the recent literature, great attention has been given to the synthesis and characterization of zeolite-based catalysts for various applications.[1] Most of the work reported is concerned with catalysts for thermal processes; however, applications of zeolite-based photocatalysts are increasingly reported in the literature.[2] The very important step of light harvesting is either achieved by using semiconductor-photocatalysts, such as (doped) titanium dioxide[3] or by incorporating organic[4] or inorganic[5] sensitizers into the zeolite's framework. The latter strategy depends on the development of synthetic "ship-in-bottle" strategies, which allows the *in-situ* synthesis of the sensitizers within the zeolites supercages.[6] The 2,4,6-triphenylpyrylium cation was employed as organic sensitizer[7] and was successfully applied for the photooxidation of pollutants, dissolved in water, such as methyl parathion[8] or propoxur.[9] Further applications of the zeolite embedded 2,4,6-triphenylpyrylium cation consist of its use as a selective electrode for the electrochemical determination of dopamine in the presence of ascorbic acid.[10] The inorganic sensitizers consist either of d-group metal cations[4] or d-group metal cations possessing organic ligand systems.[11] The synthesis of organic sensitizers within the zeolite′s supercages often enhances their light absorption properties and their lifetimes of the photoexcited states, in comparison to the photophysical properties of the corresponding d-group metal cations in (aqueous) solution.[12]

The doping of zeolite Y with $[Ru(bpy)_3]^{2+}$ has already been performed in 1980 by DeWilde, Peeters and Lunsford,[13] and during the last 22 years, many physical and photophysical studies were accomplished with $[Ru(bpy)_3]^{2+}$ doped zeolites.[14] Assuming that zeolites are insulators, electron-transfer can only occur by electron-hopping between different metal complexes or other redox-active dopands in the cavities of these materials.[15] In general, the light harvesting efficiency of zeolite-based photocatalysts containing $[Ru(bpy)_3]^{2+}$ or related compounds as photosensitizers is found to be low when there are no electron relays embedded in their structural framework.[16] The presence of electron relays within the zeolite is a necessary condition for directed electron transfer and therefore, for an enhanced charge separation. Following this paradigm, the photocatalytic treatment of waste-water was achieved

† Dedicated to the memory of Nobel Laureate, Lord George Porter FRSC FRS OM.

For part I, see ref. 19.

Electronic supplementary information (ESI) available: preliminary photolysis experiments. See http://www.rsc.org/suppdata/pp/b2/b212377k/

employing a platinized $[Ru(bpy)_3]^{2+}$ doped zeolite Y catalyst.[17] Das and Dutta doped zeolite Y encapsulated $[Ru(bpy)_3]^{2+}$ with ruthenium oxide and achieved the photochemical generation of dioxygen from water.[18] In 2001, the team from the University of Karlsruhe presented a $[Ru(bpy)_3]^{2+}/TiO_2$ codoped zeolite Y catalyst.[19] The catalysts consisted of zeolite Y-encapsulated $Ru(bpy)_3^{2+}$ (bpy = 2,2′-bipyridine) sensitizers in close proximity to TiO_2 nanoparticles on the same support. The photoexcited MLCT state of the zeolite-entrapped $Ru(bpy)_3^{2+}$* reacts *via* electron transfer with $Co(dpphen)_3^{3+}$ (dpphen = 4,7-diphenyl-1,10-phenanthroline) at the exterior of the zeolite particles. The quenching of $Ru(bpy)_3^{2+}$* by external $Co(dpphen)_3^{3+}$ increases as the TiO_2 content within the zeolite is increased. Excited $Ru(bpy)_3^{2+}$*- complexes located within the interior of the zeolite Y are able to transfer electrons to the external electron acceptor $Co(dpphen)_3^{3+}$. Principally, our results are supported by a time-resolved study of Scaiano and coworkers.[20] Both studies show that static quenching occurs between the photoexcited sensitizer and the neighboring TiO_2 (nano)particles. Slight differences in the observed photophysical behavior can be attributed to the different synthetic approaches.

After the photoelectron transfer ability of this novel class of $[Ru(bpy)_3]^{2+}/TiO_2$ codoped zeolite Y materials was successfully demonstrated, we focused our attention on a set of bench reactor experiments in order to determine their potential in Advanced Oxidation Processes (AOPs).[21] During the last decades, we have demonstrated that 2,4-xylidine is a suitable model pollutant in AOP-studies, because it permits the elucidation of the chemical nature of the oxidizing intermediate. If the hydroxyl radical is generated, 2,4-xylidine will undergo hydroxylation reactions and form aminophenols, whereas 2,4-dimethylphenol is produced, among other intermediates, if an electron transfer reaction takes place.[22] The photochemical reactivity of the $[Ru(bpy)_3]^{2+}/TiO_2$ codoped zeolite Y photocatalysts as well as the chemical nature of the intermediates formed from 2,4-xylidine was studied as a function of titanium dioxide loading. This set of experiments was designed to elucidate the percolation behavior of 2,4-xylidine through the zeolite Y′s interconnecting network.

Experimental

General procedures

All reagents and solvents used were of the highest purity available and were purchased from Aldrich and Fluka. H_2O was of triple-dest. quality (UHQ-II). X-Ray powder diffractograms have been recorded at the Institute for Mineralogy at the University of Karlsruhe (Prof. E. Althaus). Raster electron microscopy and X-ray elementary analysis (Zeiss 910) has been performed in the Laboratories for Electron Microscopy at the University of Karlsruhe (Prof. D. Gerthsen). N_2-adsorption studies according to the BET-methods have been performed at the Institute for Petrochemistry at the University of Karlsruhe (Prof. K. Griesbaum).

Luminescence spectroscopy and H_2O_2-quenching studies

Steady-state and time-resolved fluorescence measurements were performed at T = 293 K using an Edinburgh Analytical Instruments (EAI-FS/FL900) Single-Photon-Counting instrument, which is able to fit lifetimes in the range of 500 ps to 500 μs. For these experiments 10 mg of the zeolite samples were predried for 12 h at 100 °C, then 3.0 ml H_2O were added prior to each measurement. In the H_2O_2-quenching studies, the quencher was added from a stock solution (c = 2.0 M) by means of a micropipette (Eppendorf).

Photolysis experiments

The heterogeneous photolysis experiments were carried out in a bench reactor (Fig. 1).

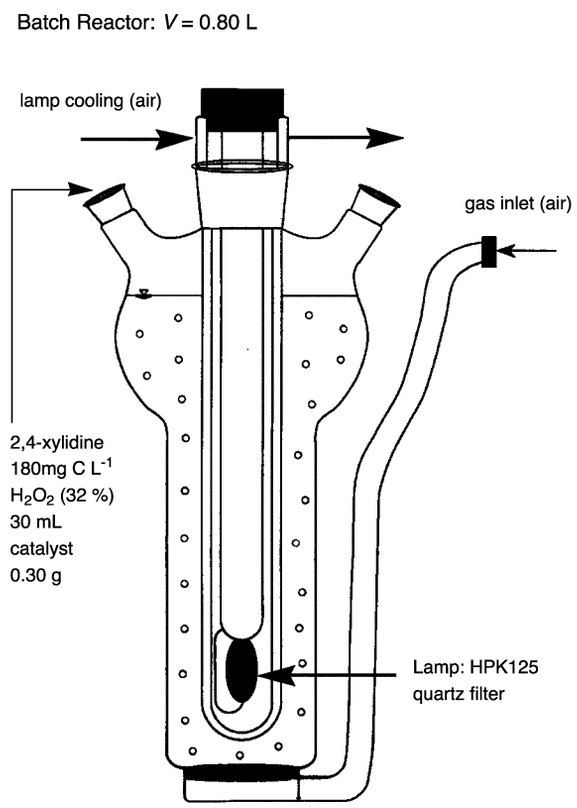

Fig. 1 Immersion type reactor for photocatalytic experiments.

The total volume of the reactor was V = 0.80 L, the total volume of the photolysis solution was V = 0.50 L (2,4-xylidine: 180 mg C L^{-1} (9.37×10^{-4} mol)). 0.30 g of the heterogeneous photo-catalysts were added before each photolysis. The pH was adjusted to the initial value of 3.0 using H_2SO_4. After 25 min of equilibration, 30 mL H_2O_2 (32 wt%, corresponding to 2.75×10^{-2} mol) was added (t_0 = 0) and the light source ignited. An additional 10 mL (9.18×10^{-3} mol) of H_2O_2 was added at exactly 30, 60, 90 and 120 min of photolysis time. The reaction system was intensively purged by compressed air. The analysis was performed immediately after taking the samples, which were filtered using Nylon Luer-Lock-membrane filters (Roth, 0.22×10^{-6} m). For quantitative HPLC-analysis an HP Series II 1090 Liquid Chromatograph, equipped with a diode-array-detector (DAD) and a LiChrospher-100 RP 18 column and precolumn were used (mobile phase: 0.10 mol L^{-1} $(C_2H_5)_3N/H_3PO_4$ (pH = 7.0)–acetonitrile, 75 : 25 v/v) for the determination of 2,4-xylidine and reaction intermediates. Total organic carbon (TOC) was measured by means of a Dohrmann DC-190-analyzer.

Results and discussion

I. Synthesis and characterization of $[Ru(bpy)_3]^{2+}/TiO_2$ codoped zeolite-Y

Zeolite Y belongs to the faujasite family. All faujasites feature typical structural principles: the first consists of building blocks of SiO_4 and AlO_4^- tetrahedrons, the second is the formation of six-membered rings formed by these tetrahedrons, and the third structural principle is the β-cage formed by the combination of four- and six-membered rings. The formula of the employed zeolite Y (Linde NaY-52) is $Na_{54.2}(Al_{54.2}Si_{137.8}O_{384})\cdot\approx 235H_2O$ (300 K, M = 16977.87 g/mol elementary cells).[23] These supercages exhibit a diameter of approximately 1.30 nm and are connected by "windows". Their widest diameter is 0.74 nm. The ratio of cavities to windows in the interior of zeolite Y is 1 : 2. The cavities form a tetrahedral lattice. Scheme 1 shows such a large cavity (supercage), the locations of the windows as well as

Table 1 Chemical composition, luminescence excitation and emission maxima and emission lifetime(s) of $Ru(bpy)_3^{2+}$ in zeolite Y under various loadings of Ru(II) complex and TiO_2

$Ru(bpy)_3^{2+}$ (wt%)[a]	TiO_2 (wt%)	λ_{em}[b]/nm	τ_1/ns	A[c]	τ_2/ns	B[c]
23.5 ± 0.4	0	613	141	70	40	30
21.7 ± 0.5	4.5 ± 0.5	650	171	83	37	17
22 ± 0.5	9.5 ± 0.5	652	278	97	67	3
23 ± 0.5	12 ± 0.5	652	253	91	64	9
23 ± 0.5	15 ± 0.5	656	231	88	61	12
23 ± 0.5	17 ± 0.5	651	228	81	59	19
23 ± 0.5	19 ± 0.5	660	224	80	62	20
23 ± 0.5	22 ± 0.5	668	248	78	63	22
23 ± 0.5	24 ± 0.5	661	219	75	57	25
23 ± 0.5	27 ± 0.5	655	205	100		
23 ± 0.5	29 ± 0.5	660	217	100		
23 ± 0.5	31.5 ± 0.5	670	227	100		
21 ± 0.5	32.5 ± 0.5	672	250	100		
21 ± 0.5	33.0 ± 0.5	670	247	100		
23 ± 0.5	34.5 ± 0.5	672	266	100		
20.5 ± 0.5	36.0 ± 0.5	672	270	100		
22 ± 0.5	37.0 ± 0.5	668	274	100		
19.5 ± 0.5	40.0 ± 1.0	671	288	100		

[a] 25.1% loading represents one $Ru(bpy)_3^{2+}$ complex in each supercage. [b] λ_{ex} = 481 ± 3 nm in all experiments. [c] Decays fit to $[A\exp(-t/\tau_1) + B\exp(-t/\tau_2)]$, the experimental error in the photophysical measurements is <± 3 rel. percent.

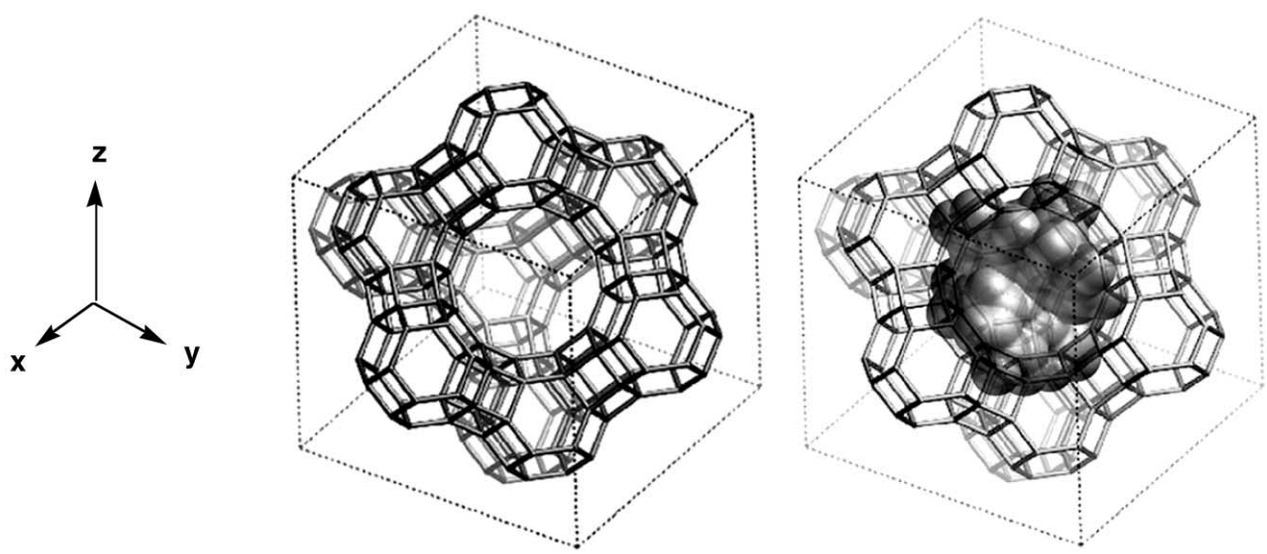

Scheme 1 Framework of zeolite Y viewed along the [111] position and geometric extension of $[Ru(bpy)_3]^{2+}$ inside the supercage.

the position and geometric extension of $[Ru(bpy)_3]^{2+}$ inside the supercage. Scheme 2 shows a schematic representation of a $[Ru(bpy)_3]^{2+}/TiO_2$ codoped zeolite Y photocatalyst.

Since $[Ru(bpy)_3]^{2+}$ has a diameter of 1.08 nm,[24] its synthesis inside the zeolite Y supercage must be performed using a "ship in bottle" approach: first, the supercages of the zeolite Y are doped with Ru^{3+} and subsequently the ligand 2,2′-bipyridine is added through the windows of the zeolite structure. The exact procedure for the synthesis of our $[Ru(bpy)_3]^{2+}$ -doped zeolite Y is published.[19] Note that we aimed to assemble one $[Ru(bpy)_3]^{2+}$ sensitizer per zeolite supercage. For technical reasons (filtration, recycling of the photocatalysts) we have employed relatively large particles of an average diameter of 1.0×10^{-6} m, hence exhibiting an average number of cavities per particle of $5 \pm 2 \times 10^8$. Our analysis of the materials, (performed by zeolite Y hydrolysis and consequent HPLC-analysis) before incorporating the titanium dioxide indicated that we almost succeeded in this goal. We have reached reaction yields of 87.5 to 92%, as summarized in Table 1. We have attributed this increased reaction yield to the use of a solvent (ethylene glycol), which leads to a better distribution and a higher diffusion of 2,2′-bipyridine than usually found in solid state syntheses, where ruthenium(III)-doped zeolite Y powder and solid 2,2′-bipyridine are mixed and then heated.

The subsequent synthesis of titanium dioxide codoped zeolite Y containing $[Ru(bpy)_3]^{2+}$ in almost every supercage was achieved by using $TiCl_3$ as the titanium source.[25] The different TiO_2 loadings of the various photocatalysts synthesized were achieved by weighing different amounts of solid $TiCl_3$ under an argon athmosphere. Again, ethylene glycol was used as solvent and dispersion agent, respectively. Ti(III) cations were able to diffuse to the surface of zeolite Y and consequently also in its interior. The following step consisted of a controlled hydrolysis of the adsorbed and absorped Ti(III) clusters at −5 to 0 °C under an air atmosphere. This was achieved by the addition of 5.0 g Na_2CO_3, dissolved in 100 mL H_2O. Note that no loss of titanium(III/IV) was observed during reaction. Consequently, very close to 100% of titanium(IV) was found to be incorporated into the zeoliteY/$[Ru(bpy)_3]^{2+}$ framework. Finally, the formed composite materials were filtered off and heated up to 200 °C in order to obtain well defined Ti(IV) nanoparticles.

I. Characterization of the $[Ru(bpy)_3]^{2+}/TiO_2$ codoped zeolite Y based photocatalysts

The results from X-ray powder diffraction, REM, TEM and differential pulse voltammography (DPV) were previously published.[19] In Table 1, the data from elementary analysis,

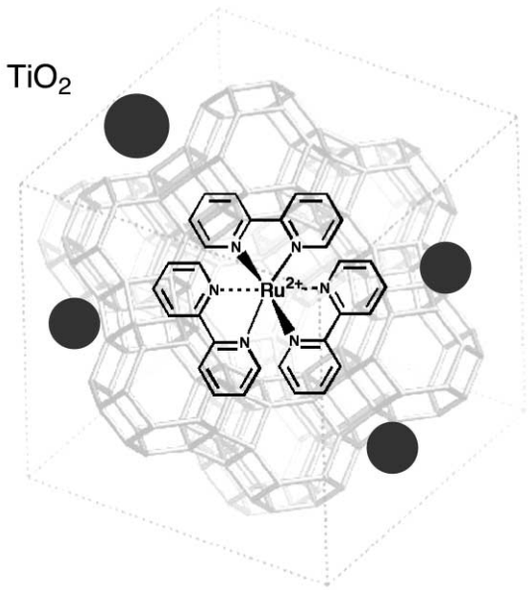

Scheme 2 Schematic representation of a $[Ru(bpy)_3]^{2+}/TiO_2$ codoped zeolite Y photocatalyst.

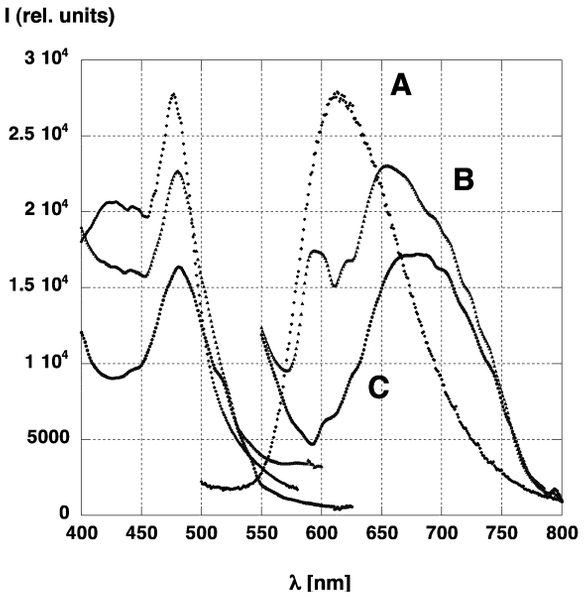

Fig. 2 Steady-state luminescence spectra (right: emission spectra, left: excitation spectra): (A) 23 ± 0.5 wt% of $[Ru(bpy)_3]^{2+}$, 0 wt% of TiO_2; (B) 22 ± 0.5 wt% of $[Ru(bpy)_3]^{2+}$, 9.5 wt% of TiO_2; (C) 23 ± 0.5 wt% of $[Ru(bpy)_3]^{2+}$, 34.5 wt% of TiO_2.

steady-state and time-resolved luminescence spectroscopy are summarized. A part of this data was shown already in ref. 19. As it becomes clear from Table 1, we were able to increase the titanium dioxide content of the heterogeneous photocatalysts to up to 40 wt%. However, the ruthenium content, determined using ICP, only decrease at the highest TiO_2 loadings. This puzzling result can be regarded as an indication of the following processes occurring during $TiCl_3$-exchange and oxidative hydrolysis: (1) zeolite-bound water reacts either with $TiCl_3$ or is displaced by the growing TiO_2 (nano)particles. (2) A consequent de-alumination of zeolite Y during synthesis is likely. In agreement with this hypothesis, the crystallinity of the $[Ru(bpy)_3]^{2+}/TiO_2$ codoped zeolite Y based photocatalysts decreased stepwise from 98% for $[Ru(bpy)_3]^{2+}$ doped zeolite Y to 41% for the material with the highest TiO_2 loading (40 wt%).

The luminescence occurring from the $[Ru(bpy)_3]^{2+}/TiO_2$ codoped zeolite Y based photocatalysts during steady-state irradiation was analyzed together with the corresponding excitation spectra. The results are summarized in Table 1. Three typical examples are shown in Fig. 2. Note that the luminescence bands of the photocatalysts with incorporated TiO_2 (nano)particles are found to be very broad, possessing half-widths larger than 100 nm. In the absence of TiO_2, the luminescence arising from $[Ru(bpy)_3]^{2+}*$ (λ_{ex} = 480 nm, λ_{em} = 613 nm) within the zeolite's supercage was very similar to $[Ru(bpy)_3]^{2+}*$ in aqueous solution.[24] This observation is, principally, in agreement with earlier findings.[20] With increasing TiO_2 contents however, an increased red-shift of the luminescence could be detected. The excitation and emission maxima shifted to λ_{ex} = 482 nm, λ_{em} = 652 nm at respectably lower TiO_2 loadings (9.5 wt%), to finally λ_{ex} = 482 nm, λ_{em} = 672 nm, respectably, at a TiO_2 content of 40%. This red-shift in luminescence corresponds to the previously observed red-shift in UV/Vis-absorption[19] and is also consistent with the observed shift of the oxidation potential of the $[Ru(bpy)_3]^{2+}$ in the presence of TiO_2. All these effects are indicative of an electronic coupling between the $[Ru(bpy)_3]^{2+}$ complexes and TiO_2 nanoparticles synthesized inside zeolite Y.[19]

II. Photocatalytic properties: the Fenton-type-reaction using the sensitizer $[Ru(bpy)_3]^{2+}$ for the photo-enhanced degradation of 2,4-xylidine in the presence of TiO_2 nanoparticles

Quenching of $[Ru(bpy)_3]^{2+}*$ by TiO_2. It is our goal to achieve a detailed mechanistic understanding of the photochemical processes occurring in our codoped heterogeneous photocatalysts. The first step toward this challenge consists in the measurement of the quenching effect of TiO_2 (nano)particles, which were, at least partially, synthesized in direct proximity to the $[Ru(bpy)_3]^{2+}$ sensitizers inside the zeolite's supercages. According to the results independently obtained by Scaiano and coworkers[20] and our group,[19] the electron transfer quenching between $[Ru(bpy)_3]^{2+}*$ and TiO_2 appears to be static. In Fig. 3, a Stern–Volmer plot of the integrated luminesence intensity in the wavelength range from 600 to 800 nm is presented. It becomes immediately clear that (a) the observed quenching is relatively weak and (b) two distinct regions exist. At lower TiO_2 quantities (0–27.5 wt%) the quotient I^0/I increases linearly with increasing TiO_2 content. The quenching rate constant was evaluated to $k_q \approx 1.6 \times 10^{-5}\ \%^{-1}\ s^{-1}$. ‡ This finding suggests that

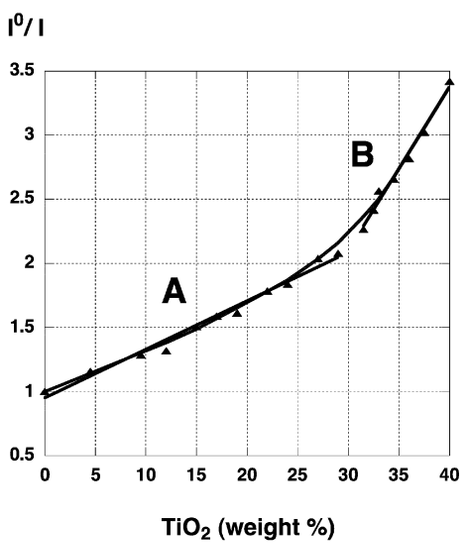

Fig. 3 Stern–Volmer plot of the quenching of $[Ru(bpy)_3]^{2+}*$ by the TiO_2 content of the codoped photocatalysts, plotted as wt% TiO_2 *vs.* I^0/I (10 mg in H_2O).

‡ Note that the observed luminescence lifetimes of the various $[Ru(bpy)_3]^{2+}/TiO_2$ codoped zeolite Y based photocatalysts vary (see Table 1). Therefore, a proper quenching rate constant cannot be obtained.

the number of titanium dioxide nanoparticles, which were formed in direct proximity of $[Ru(bpy)_3]^{2+}$ during synthesis (so that static quenching can take place) increases in this range.[26] Beyond a TiO_2 content of 30 wt%, the quotient I^0/I was found to be curving upwards distinctly. Most likely, this enhanced static quenching is caused by the presence of more than one TiO_2 particle, embedded in the zeolite's superstructure, within the diffusion range of an excited $[Ru(bpy)_3]^{2+}$*complex. An approximate quenching constant for that region was determined to be $k_q \approx 5.1 \times 10^{-5}$ $\%^{-1}$ s^{-1}. Since the diameter of $[Ru(bpy)_3]^{2+}$ ($d = 1.08$ nm)[24] is smaller than that of the zeolite Y supercage ($d = 1.30$ nm), there is, especially in the presence of H_2O within the zeolite's framework, a sufficient mobility of $[Ru(bpy)_3]^{2+}$*, permitting frequent collisions with the wall regions. The latter host the TiO_2 (nano)particles presumably, which then act as static quenchers.

Quenching of $[Ru(bpy)_3]^{2+}$* by H_2O_2. Our preliminary photolysis (see ESI†) experiments show that, neither $[Ru(bpy)_3]^{2+}$ doped zeolite Y nor the $[Ru(bpy)_3]^{2+}/TiO_2$ codoped photocatalysts were efficient in the degradation of 2,4-xylidine. Therefore we decided to add hydrogen peroxide (H_2O_2) in order to obtain a (photochemically enhanced) Fenton-type reaction system.[22]

The next logical step in our investigation consisted in the elucidation of the quenching effect of H_2O_2 on the luminescence from $[Ru(bpy)_3]^{2+}$* in dependence of the TiO_2 loading of the heterogeneous photocatalysts. As it can be seen from Fig. 4(A), which shows a typical example (9.5 wt% of TiO_2), the slope of the resulting Stern–Volmer plots were linear. The quenching effect caused by the addition of H_2O_2 to the $[Ru(bpy)_3]^{2+}/TiO_2$ codoped photocatalysts was found to be in the range of $k_q = 0.177 \pm 0.001$ M^{-1} s^{-1} (measured for 0% TiO_2) to $k_q = 2.335 \pm 0.005$ M^{-1} s^{-1} (obtained for 34.5 wt% of TiO_2).

A plot of the quenching rate constant (luminescence quenching by H_2O_2) k_q/M^{-1} s^{-1} *vs.* the TiO_2 content (Fig. 4(B)) reveals that the reactivity of the $[Ru(bpy)_3]^{2+}/TiO_2$ codoped photocatalysts with hydrogen peroxide generally follows a percolation behavior;[27] the lowest quenching rate constant can be found in the absence of TiO_2 (nano)particles in the zeolite framework. The observed quenching rate constants increase with rising TiO_2 content until a distinct maximum is reached, and then decrease with further increasing TiO_2 content.

This effect can be attributed to the presence of the TiO_2 (nano)particles, which are deposited during synthesis, in a manner so that they block the "window" regions in the zeolite's interior. These "windows" interconnect the supercages where the $[Ru(bpy)_3]^{2+}$ sensitizers are located. Through these "windows" ($d = 0.74$ nm) H_2O_2 can reach the zeolite-encapsulated sensitizers. However, if these "windows" are blocked by TiO_2 (nano)particles, the excited $[Ru(bpy)_3]^{2+}$ sensitizers cannot be reached by the H_2O_2. Consequently no quenching can be observed. On the other hand, in the presence of TiO_2 the quenching of $[Ru(bpy)_3]^{2+}$* is remarkably enhanced (by a factor up to 13 when we compare the quenching rate constants in the absence and at the maximum loading of TiO_2). Therefore, the increase in the number of accessible TiO_2 (nano)particles leads to the observed increase in the quenching rate constants before their blocking-effect limits the diffusion of H_2O_2 into the interior of the codoped zeolite, and then the quenching of $[Ru(bpy)_3]^{2+}$* by H_2O_2 decreases.

On the basis of this experimental data, the following paradigm for the photoinduced reactivity inside the codoped photocatalysts was developed:

$[Ru(bpy)_3]^{2+}$* can be quenched directly by H_2O_2. However, this reaction is relatively slow (see above). According to the literature,[28] the quenching can proceed under electron transfer from $[Ru(bpy)_3]^{2+}$* to H_2O_2 (eqn. (1)).

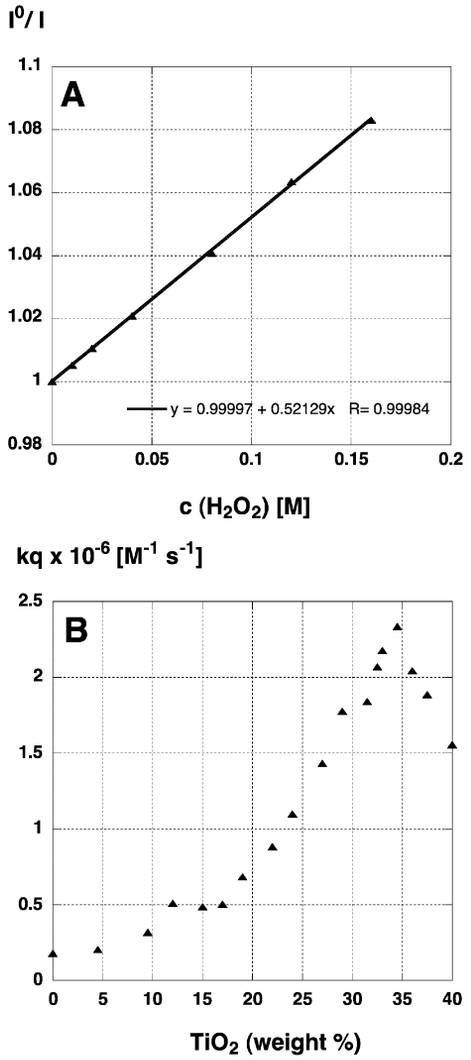

Fig. 4 (A) Stern–Volmer plot of a zeolite Y based photocatalysts (22 ± 0.5 wt% of $[Ru(bpy)_3]^{2+}$, 9.5 wt% of TiO_2, quenched by H_2O_2. (B) Plot of the quenching constant k_q/M^{-1} s^{-1} of $[Ru(bpy)_3]^{2+}$* by H_2O_2 *vs.* the TiO_2 content (wt%).

$$[Ru(bpy)_3]^{2+}* + H_2O_2 \longrightarrow [Ru(bpy)_3]^{3+} + HO^{\bullet} + HO^{-} \quad (1)$$

The hydroxyl radical ($E_{ox}(HO^{\bullet}_{aq}/H_2O_{aq}) = 2.59$ V *vs.* SHE (pH = 0)[29]) is formed, which acts as highly reactive intermediate in many AOPs.[21] The photooxidized complex $[Ru(bpy)_3]^{3+}$ ($E^0(Ru^{2+/3+}) = 1.28$–1.31 V *vs.* SHE) undergoes a thermal electron transfer reaction with excess H_2O_2 ($E_{ox}(H_2O_{2aq}/O_2) = 0.682$ V *vs.* SHE (pH = 0)[29]). In this reaction the hydroperoxyl radical is generated ($HO_2^{\bullet}$), which may participate in a manifold of thermal reactions.[21]

$[Ru(bpy)_3]^{2+}$* can apparently be quenched more efficiently by H_2O_2, when TiO_2 (nano)particles act as electron relays. From the comparison of the luminescence behavior in the absence and the presence of TiO_2, we have developed the following reaction sequence: The first step consists in the chemisorption of freely diffusing H_2O_2 at the surface of the TiO_2 (nano)particles (eqn. (2.1)). The adsorption of H_2O_2 at TiO_2 enhances the rate of photoinduced electron transfer between $[Ru(bpy)_3]^{2+}$* and H_2O_2 ((eqn. 2.2)). As discussed above, $[Ru(bpy)_3]^{2+}$ and also $[Ru(bpy)_3]^{2+}$* possess a definite degree of mobility inside the zeolite Y supercage and can, therefore, bounce against TiO_2 (nano)particles inside or at the boundaries of the supercages. Based on the weak quenching of $[Ru(bpy)_3]^{2+}$* by TiO_2, we concluded that not every collision between $[Ru(bpy)_3]^{2+}$* and TiO_2 leads to a successful electron transfer event. The chemisorption of H_2O_2

at TiO_2 enhances apparently the probability of electron transfer during such a collision. This effect leads to an improvement of electron transfer quenching of $[Ru(bpy)_3]^{2+}$* by TiO_2. After electron transfer has taken place, the injected electron is transmitted through the valence band to H_2O_2 and causes the generation of a hydroxyl radical, which remains chemisorbed at TiO_2 by means of eqn (2.3).

(2.1)

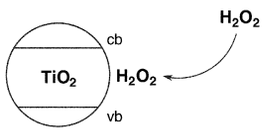

(2.2)

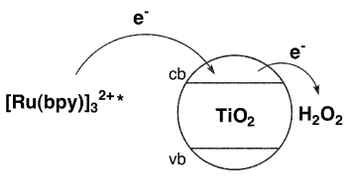

(2.3)

$$TiO_2(e^-) + H_2O_{2,ads} \longrightarrow TiO_2 + HO^{\cdot}_{ads} + HO^-$$

Photooxidation of the model pollutant 2,4-xylidine by $[Ru(bpy)_3]^{2+}/TiO_2$ codoped zeolite Y based photocatalysts in a bench reactor. In order to perform a test of the photocatalytic properties of our novel photocatalysts, 2,4-xylidine has been chosen as the model pollutant. As discussed in the Introduction, this model compound is of great importance as far as applied research is concerned. The oxidation experiments have been performed in a bench reactor (V = 500 mL); a mercury medium pressure lamp (HPK, quartz filter) was employed as light source (see Fig. 1). The 2,4-xylidine starting concentration was equivalent to 180 ppm C (9.37×10^{-4}) mol, and then 0.30 g of the heterogeneous photocatalysts have been added. All photolysis suspensions were adjusted to pH = 3.0 by addition of H_2SO_4 (1.0 M). After exactly 25 min of equilibration, 30 mL H_2O_2 (32 wt%) was added at $t = 0$ and the light source switched on. An additional 10 mL of H_2O_2 were added at exactly 30, 60, 90 and 120 min of photolysis time. The reaction system was intensively purged by compressed air.

In Fig. 5, the photooxidations of 2,4-xylidine by two $[Ru(bpy)_3]^{2+}/TiO_2$ codoped zeolite Y photocatalysts possessing a TiO_2 content of 9.5 wt% (A) and 34.5 wt% (B), respectively, are compared. In both cases, the concentration of 2,4-xylidine decreases much faster than the DOC (dissolved organic carbon), which was monitored to obtain information about the mineralization processes occurring in the photoreactor. A more detailed HPLC analysis of the reaction intermediates (see below) revealed that the major product from the oxidation of 2,4-xylidine was oxalic acid. It becomes clear from Fig. 5 that the further oxidation of oxalic acid to carbon dioxide is very sluggish under our conditions, because the main intermediate oxalic acid cannot be retained and further oxidized by the heterogeneous photocatalyst. However, the resulting aqueous solutions contain no aromatic hydrocarbons, but only oxalic acid and other aliphatic carboxylic acids. These solutions can be easily treated further in municipal water remediation plants, because they are no longer toxic!

Because the pH of the solution outside the zeolite particles is 3.0, our model compound 2,4-xylidine forms the xylidinium ion $[Hxyl]^+$ at the exterior side of the zeolite's framework. $[Hxyl]^+$ enters the zeolite framework through the "windows". According to results from simple molecular modeling, both, $[Hxyl]^+$ and $[Ru(bpy)_3]^{2+}$ fit together in one zeolite Y supercage.§ In the interior of zeolite Y (3 > pH > 7),[30] the xylidinium ion is deprotonated and forms the neutral organic compound 2,4-xylidine, which can also percolate through the zeolite structure. There is a detectable loss of dissolved organic carbon (DOC) before the ignition of the mercury medium pressure lamp, which can be explained by the absorption of 2,4-xylidine within the codoped zeolite Y. The ability of $[Hxyl]^+$ to percolate through the zeolite Y's superstructure strongly depends on the availability of open "windows". The reaction rates of initial 2,4-xylidine disappearance were obtained from the plot of $-\ln(c_0/c)$ *vs.* t. Their dependence on the TiO_2 content of the codoped photocatalysts is shown in Fig. 6.

The data summarized in Fig. 6 represents a typical percolation behavior, as already found for the quenching of $[Ru(bpy)_3]^{2+}$* by H_2O_2 (see Fig. 4). The presence of TiO_2 (nano)particles greatly enhances the photocatalytic activity of

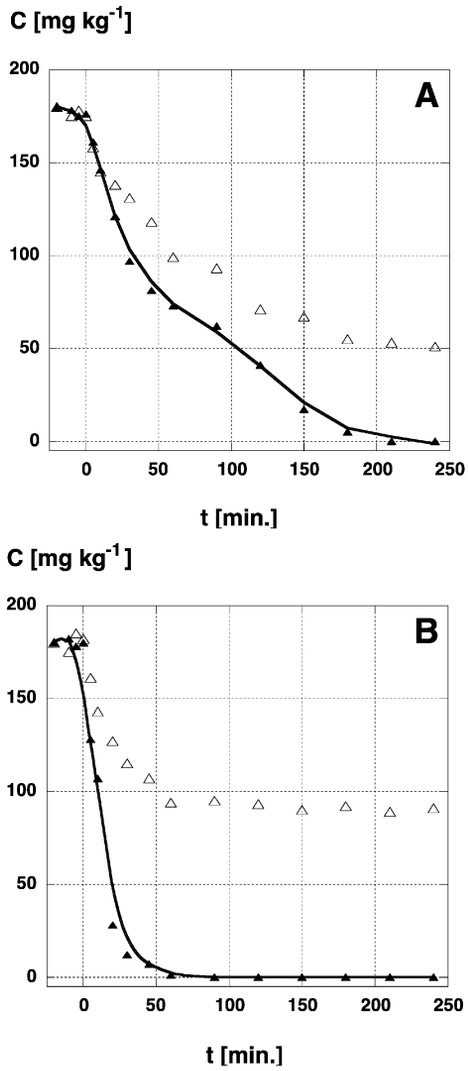

Fig. 5 (A) Photochemically enhanced $[Ru(bpy)_3]^{2+}$ Fenton-type reaction: 0.50 L of an aqueous 2,4-xylidine solution (180 ppm C, pH = 3.0, 0.30 g photocatalyst (22 ± 0.5 wt% of $[Ru(bpy)_3]^{2+}$, 9.5 wt% of TiO_2), H_2O_2 (30 mL (32 wt%) at $t = 0$ min + 10 mL H_2O_2/30 min); filled triangles: 2,4-xylidine, open triangles: DOC. (B) Photochemically enhanced $[Ru(bpy)_3]^{2+}$ Fenton-type reaction: 0.50 L of an aqueous 2,4-xylidine solution (180 ppm C, pH = 3.0, 0.30 g photocatalyst (23 ± 0.5 wt% of $[Ru(bpy)_3]^{2+}$, 34.5 wt% of TiO_2), H_2O_2 (30 mL (32 wt%) at $t = 0$ min + 10 mL H_2O_2/30 min); filled triangles: 2,4-xylidine, open triangles: DOC.

§ Chemdraw 3D was used to estimate the van der Waals radii of $[Ru(bpy)_3]^{2+}$, $[Hxyl]^+$ and 2,4-xylidine.

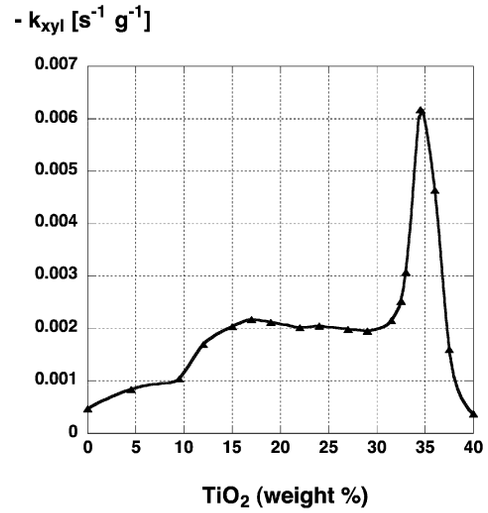

Fig. 6 Plot of the rate constant of initial 2,4-xylidine disappearance ($-k_{xyl}$/s^{-1} g^{-1}) *vs.* the TiO_2 content (wt%).

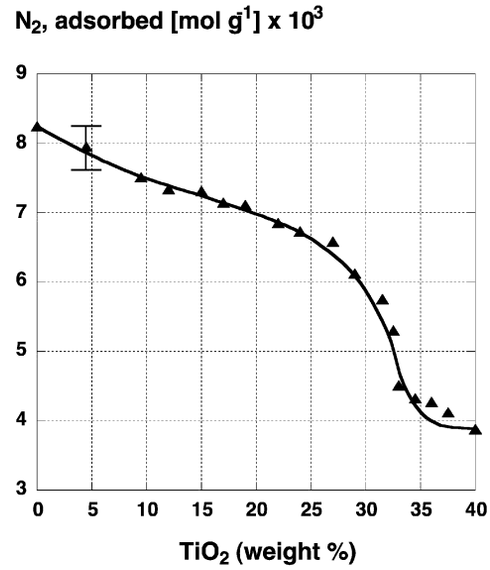

Fig. 7 Plot of the amounts of N_2/mol g^{-1}, adsorbed at 77 K, *vs.* the TiO_2 content (wt%) of the photocatalysts.

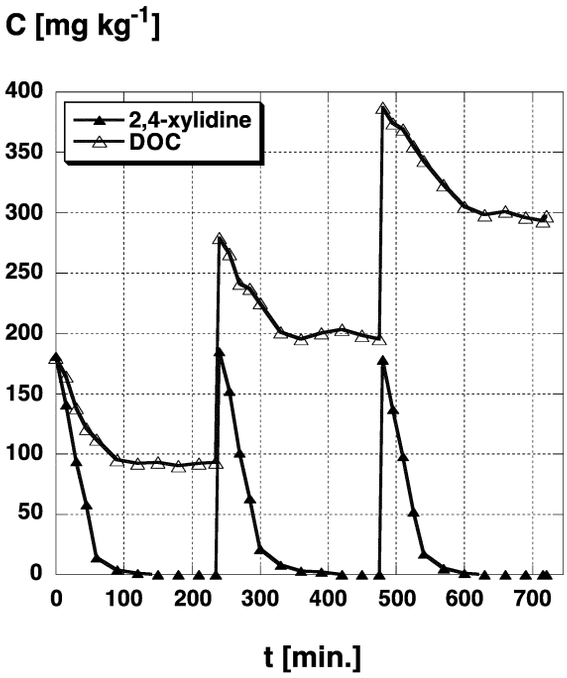

Fig. 8 2,4-Xylidine injection (equivalent of 180 ppm [C] each) at $t = 0$, 240 and 480 min 0.50 L of an aqueous solution, pH = 3.0, 0.30 g photocatalyst (23 ± 0.5 wt% of $[Ru(bpy)_3]^{2+}$, 34.5 wt% of TiO_2), H_2O_2 (30 mL (32 wt%) at $t = 0$ min + 10 mL H_2O_2/30 min).

the heterogeneous photocatalysts. On the other hand, if the TiO_2 (nano)particles block the "windows" increasingly, the photocatalytic activity of the codoped photocatalysts reaches a maximum and then decreases, because the diffusion of $[Hxyl]^+$ inside the zeolite Y becomes increasingly difficult. Unfortunately, the microkinetics of these processes are occurring inside the framework of zeolite Y and exact data about the blocking of "windows" by TiO_2 (nano)particles are not yet available. Therefore, we abandoned the attempt to fit these data to a specific percolation model. However, the prevalence of percolation conditions is evident. Further support for this mechanistic explanation comes from the measurements of adsorbed N_2 as a function of TiO_2 loading of the zeolite Y/$[Ru(bpy)_3]^{2+}$/TiO_2 photocatalysts. Since classic BET analysis[31] cannot be employed for the investigation of zeolites because important mechanistic prerequisites are not met if zeolites are investigated,[32] we did not establish typical BET-parameters such as BET-surfaces (accessible for N_2 at its boiling temperature), but rather compared the volumes of zeolite Y/$[Ru(bpy)_3]^{2+}$/TiO_2 adsorbed N_2 (Fig. 7). For zeolite Y/$[Ru(bpy)_3]^{2+}$ 0.0082 mol N_2 per g of photocatalyst were measured. The plot of the molar amounts of adsorbed N_2 as a function of the TiO_2 loadings reveals a sharp drop in the region between 29 and 37.5%, where the highest photocatalytic efficiency was observed. We attribute this decrease in the N_2-adsorption to the blocking effect of zeolite Y pores by TiO_2. The final value was 0.0039 mol N_2, found at a TiO_2 loading of 40%.

The long-term stability of the photocatalyst systems is of importance. In Fig. 8, first results in this respect are presented: 2,4-xylidine was injected three times at $t = 0$, 240 and 480 min during continuous irradiation. Each time, the oxidation of 2,4-xylidine proceeded with a comparable reaction rate. The following rate constants were calculated: $-k^1_{xyl} = 0.00618$ s^{-1} g^{-1}, $-k^2_{xyl} = 0.00603$ s^{-1} g^{-1}, $-k^3_{xyl} = 0.00612/s^{-1}$ g^{-1}.

Whereas 2,4-xylidine was oxidatively degraded after each injection, the DOC rose after each injection. Again, the DOC remaining after the disappearance of 2,4-xylidine could be mainly attributed to the presence of oxalic acid as well as other aliphatic carboxylic and dicarboxylic acids. A straightforward interpretation of this finding is that oxalic acid becomes deprotonated at the higher pH inside zeolite Y, where this carboxylic acid is formed among other oxidation products. The formed oxalate anion is doubly negatively charged. Thus, charge repulsion occurs between the oxalate anion and the negatively charged framework of zeolite Y at $3 < pH < 7$. Therefore, oxalate is rapidly departing from zeolite Y and cannot enter efficiently once it reaches the aqueous phase outside the heterogeneous photocatalyst. In accordance with this hypothesis, we observed an additional DOC plateau region after each 2,4-xylidine injection.

Mechanistic considerations

As already pointed out in the Introduction, 2,4-xylidine proves to be a very valuable model pollutant, because its intermediates during oxidative degradation permit the elucidation of the prevailing oxidation mechanism.[22] In Fig. 9, the result of the HPLC-analysis of the oxidative degradation of 2,4-xylidine in our heterogeneous photocatalytic system (TiO_2 content: 17.5 wt%) is shown.

It appears that only very few reaction products are detectable. Note that several semiquinones and quinones, which were found in trace amounts, are omitted, because they do not

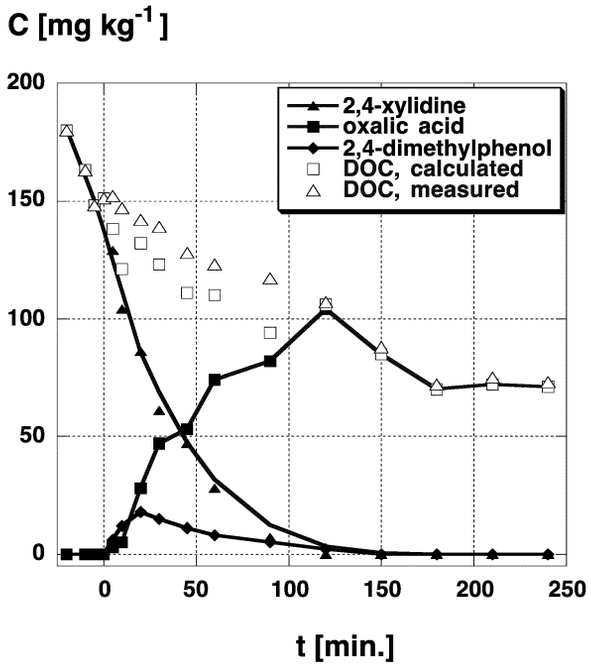

Fig. 9 Reaction intermediates of the photochemically enhanced $[Ru(bpy)_3]^{2+}$ Fenton-type reaction: 0.50 L of an aqueous 2,4-xylidine solution (180 ppm C, pH = 3.0, 0.30 g photocatalyst (23 ± 0.5 wt% of $[Ru(bpy)_3]^{2+}$, 17.5 wt% of TiO_2), H_2O_2 (30 mL (32 wt%) at t = 0 min + 10 mL H_2O_2/30 min).

account for an amount which causes a visible change in the calculated DOC. The main intermediates were 2,4-dimethylphenol and, again, oxalic acid. There is a slight difference between the measured DOC and the DOC calculated from the concentrations of 2,4-xylidine and oxalic acid in the time interval from 10 to 90 min, which clearly exceeds the limits of error of our analyses. The experimental error was determined to be smaller than ± 8 rel.% for DOC-measurements and smaller than ± 3 rel.% for the HPLC-results. The chemical nature of the identified intermediates was verified by co-injection using commercially available compounds.

In analogy to the mechanism developed for the elucidation of the key reactions of the thermal and photochemically enhanced Fenton reaction,[21] we propose the reaction sequence shown in Scheme 3: the first step was already discussed (see reaction (2.1)): (A) photoexcited $[Ru(bpy)_3]^{2+}$* reacts with H_2O_2 using the TiO_2 (nano)particles as electron relays thus generating a hydroxyl radical and a hydroxide anion. (B) The formed hydroxyl radical oxidizes the 2,4-xylidinium cation, which possesses two distinct oxidation waves at 0.670 and 0.760 V (*vs.* SHE) in acidic aqueous solution (pH = 3).[21] This oxidation takes place *via* an electron transfer reaction between the TiO_2 adsorbed hydroxyl radical and the 2,4-xylidinium cation. It is known that hydroxyl radicals can principally undergo three different types of reaction with an organic target: hydrogen abstraction, addition to double bonds, or electron transfer.[29] If the hydroxyl radical can diffuse freely, hydrogen abstraction and addition are favored and therefore numerous reaction intermediates, among them hydroxylated aromatic amines, are formed in the presence of 2,4-xylidine. For instance, hydroxylated aromatic amines are found when 2,4-xylidine is oxidized in the process of H_2O_2 photolysis.[21] These typical intermediates of the hydroxyl radical oxidation of 2,4-xylidine were also obtained when intermediate peroxyl radicals make a significant contribution to the manifold of AOP processes.[33] Instead of many intermediates, we observe exclusively 2,4-dimethylphenol as first intermediate in the degradation of the 2,4-xylidine inside the zeolite Y framework. The formation of 2,4-dimethylphenol is typical for an AOP-mechanism involving 2,4-xylidine as starting material, which proceeds exclusively *via* an electron transfer reaction. In order to compete successfully, electron transfer must be faster than hydrogen abstraction or addition. The detection of 2,4-dimethylphenol as first and only intermediate allows the mechanistic conclusion that the hydroxyl radical generated in step A must be adsorbed at the surface of the zeolite embedded TiO_2 (nano)particles during its lifetime, because it can only react *via* electron transfer! (C) The last step consists in the completion of the 2,4-xylidine mineralization. $[Ru(bpy)_3]^{3+}$ was generated during the photooxidation $[Ru(bpy)_3]^{2+}$* in step A. This Ru(III) complex can also participate in (thermal) electron transfer reactions, leading eventually to the formation of oxalic acid or mineralization. $[Ru(bpy)_3]^{3+}$ further participates in the oxidation of the aromatic amine group of 2,4-xylidine to hydroxylamine, which is then leaving the aromatic hydrocarbon. These electron transfer reactions are of importance for the regeneration of the heterogeneous photocatalysts, because $[Ru(bpy)_3]^{2+}$ is formed again by one-electron reduction of $[Ru(bpy)_3]^{3+}$.

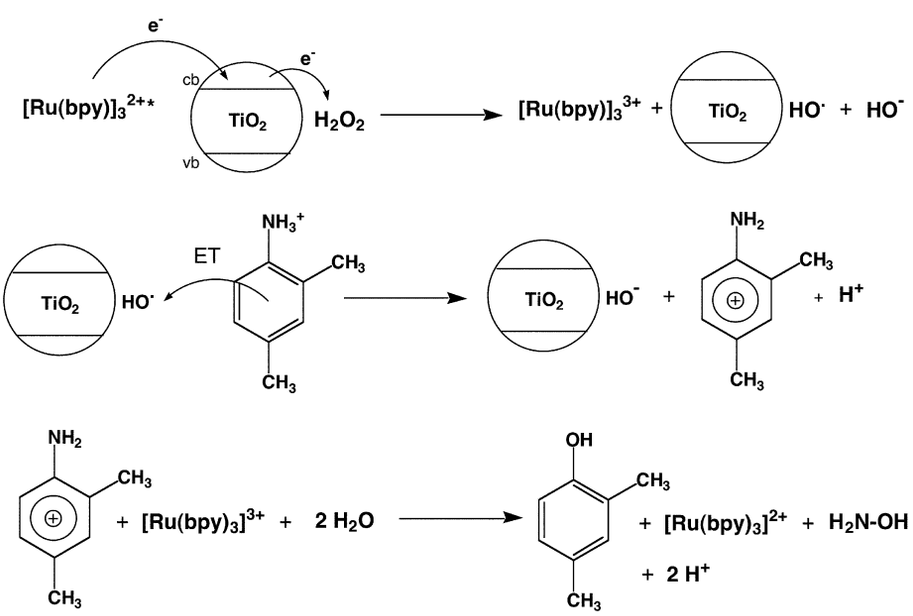

Scheme 3 Mechanistic key steps during the oxidation of the 2,4-xylidinium cation.

Conclusion

We have successfully employed a group of $[Ru(bpy)_3]^{2+}/TiO_2$ codoped zeolite Y based photocatalysts for the catalytic oxidation of the model pollutant 2,4-xylidine by H_2O_2 in a bench reactor. In accordance with the chemical nature of the hosting zeolite Y, percolation behavior was found for the luminescence quenching of $[Ru(bpy)_3]^{2+}*$ by H_2O_2 and for the oxidation of 2,4-xylidine by H_2O_2 under continuous irradiation. Our experiments led to the conclusion that zeolite-embedded TiO_2 (nano)particles play an important role in the degradation mechanism of the organic model pollutant. In the first step, H_2O_2 is adsorbed at the zeolite-embedded TiO_2 (nano)-particles.

Photoexcited $[Ru(bpy)_3]^{2+}*$ reacts in the second step with the TiO_2 adsorbed H_2O_2. The TiO_2 nanoparticles act as catalysts in this process and transmit the photo-generated electrons *via* the conduction band to H_2O_2. At the surface of TiO_2, H_2O_2 reacts then with the electron under formation of an adsorbed hydroxyl radical ($HO^{\bullet}$) and a hydroxide anion. The TiO_2 adsorbed $HO^{\bullet}$ radical reacts *via* electron transfer with the model pollutant 2,4-xylidine. This reaction behavior is indicated by the exclusive formation of 2,4-dimethylphenol as first reaction intermediate. $[Ru(bpy)_3]^{3+}$, which is produced in the photoelectron transfer reaction between $[Ru(bpy)_3]^{2+}*$ and TiO_2, can participate in the oxidation of the model pollutant. The latter process occurs also by electron transfer and leads to the recycling of $[Ru(bpy)_3]^{2+}$. The relatively high reaction rate constants found for the photooxidation of 2,4-xylidine can be attributed to suitable electron transfer conditions inside $[Ru(bpy)_3]^{2+}$ and TiO_2 codoped zeolite Y.

Acknowledgments

The authors are grateful to the NATO (CRG 940663) and the Foundation of the German Chemical Industry (VCI) and the German Research Council (DFG, BO-1060/3-3) for the financial support of this scientific collaboration. The authors at Columbia University thank the MRSEC Program of the National Science Foundation for support of this work under Award Number DMR-0213574.

References

1 (*a*) C. Schuster, E. Mollmann, A. Tompos and W. F. Holderich, Highly stereoselective epoxidation of (−)-α-pinene over chiral transition metal (salen) complexes occluded in zeolitic hosts, *Catal. Lett.*, 2001, **74**, 69–75; (*b*) S. Seelan, D. Srinivas, M. S. Agashe, N. E. Jacob and S. Sivasanker, Effects of molecular confinement on structure and catalytic behavior of metal phthalocyanine complexes encapsulated in zeolite-Y, *Stud. Surf. Sci. Catal.*, 2001, **135**, 1194–1201; (*c*) M. R. Maurya, S. J. J. Titinchi, S. Chand and I. M. Mishra, Zeolite-encapsulated Cr(III), Fe(III), Ni(II), Zn(II) and Bi(III) salen complexes as catalysts for the decomposition of H_2O_2 and oxidation of phenol, *J. Mol. Catal. A: Chem.*, 2002, **180**, 201–209; (*d*) J. Trissa, D. P. Sawant, C. S. Gopinath and S. B. Halligudi, Zeolite encapsulated ruthenium and cobalt Schiff base complexes catalyzed allylic oxidation of α-pinene, *J. Mol. Catal. A: Chem.*, 2002, **184**, 289–299.

2 W. F. Holderich, H. H. Wagner and M. H. Valkenberg, Immobilized catalysts and their use in the synthesis of fine and intermediate chemicals, *Spec. Publ. R. Soc. Chem.*, 2001, **266**, 76–93.

3 E. P. Reddy, L. Davydov and P. G. Smirniotis, Characterization of Titania Loaded V-, Fe-, and Cr-Incorporated MCM-41 by XRD, TPR, UV-vis, Raman, and XPS Techniques, *J. Phys. Chem. B*, 2002, **106**, 3394–3401.

4 S. Sinlapadech, R. M. Krishna, Z. Luan and L. Kevan, Photoionization of N-alkylphenothiazines in Mesoporous Me-AlMCM-41 Containing Transition Metal Ions Me = Ni(II), Fe(III), and Cu(II), *J. Phys. Chem. B.*, 2001, **105**, 4350–4355.

5 L. Davydov, E. P. Reddy, P. France and P. G. Smirniotis, Transition-Metal-Substituted Titania-Loaded MCM-41 as Photocatalysts for the Degradation of Aqueous Organics in Visible Light, *J. Catal.*, 2001, **203**, 157–167.

6 P. Laine, M. Lanz and G. Calzaferri, Limits of the in situ Synthesis of Tris(2,2′-bipyridine)ruthenium(II) in the Supercages of Zeolite Y, *Inorg. Chem.*, 1996, **35**, 3514–3518.

7 (*a*) A. Sanjuan, M. Alvaro, G. Aguirre, H. Garcia and J. C. Scaiano, Intrazeolite Photochemistry. 21. 2,4,6-Triphenylpyrylium Encapsulated inside Zeolite Y Supercages as Heterogeneous Photocatalyst for the Generation of Hydroxyl Radical, *J. Am. Chem. Soc.*, 1998, **120**, 7351–7352; (*b*) A. Sanjuan, M. Alvaro, G. Aguirre and H. Garcia, 2,4,6-Triphenylpyrylium ion encapsulated in Y zeolite as photocatalyst. A co-operative contribution of the zeolite host to the photodegradation of 4-chlorophenoxyacetic acid using solar light, *Appl. Catal., B: Environ.*, 1998, **15**, 247–257; (*c*) A. Domenech, M. T. Domenech-Carbo, H. Garcia and M. S. Galletero, Electrocatalysis of neurotransmitter catecholamines by 2,4,6-triphenylpyrylium ion immobilized inside zeolite Y supercages, *Chem. Commun.*, 1999, **21**, 2173–2174.

8 A. Sanjuan, G. Aguirre, M. Alvaro and H. Garcia, 2,4,6-Triphenylpyrylium ion encapsulated within Y zeolite as photocatalyst for the degradation of methyl parathion, *Water Res.*, 1999, **34**, 320–326.

9 A. Sanjuan, G. Aguirre, M. Alvaro, H. Garcia and J. C. Scaiano, Degradation of propoxur in water using 2,4,6-triphenylpyrylium-Zeolite Y as photocatalyst. Product study and laser flash photolysis, *Appl. Catal., B: Environ.*, 2000, **25**, 257–265.

10 A. Domenech, H. Garcia, M. T. Domenech-Carbo and M. S. Galletero, 2,4,6-Triphenylpyrylium Ion Encapsulated into Zeolite Y as a Selective Electrode for the Electrochemical Determination of Dopamine in the Presence of Ascorbic Acid, *Anal. Chem.*, 2002, **74**, 562–569.

11 (*a*) S. Fukuzumi, Y. Yoshida, T. Urano, T. Suenobu and H. Imahori, Extremely Slow Long-Range Electron Transfer Reactions Across Zeolite-Solution Interface, *J. Am. Chem. Soc.*, 2001, **123**, 11331–11332; (*b*) V. Ganesan and R. Ramaraj, Extrazeolite Electron Transfer at Zeolite-Encapsulated Polypyridyl Metal Complex Coated Electrodes, *Langmuir*, 1998, **14**, 2497–2501.

12 (*a*) J.-S. Hwang, D. S. Kim, C. W. Lee and S.-E. Park, Photocatalytic activation of CO_2 under visible light by rhenium complex encapsulated in molecular sieves, *Korean J. Chem. Eng.*, 2001, **18**, 919–923; (*b*) D. Rong, H. G. Hong, Y. I. Kim, J. S. Krueger, J. E. Mayer and T. E. Mallouk, Electrochemistry and photoelectrochemistry of transition metal complexes in well-ordered surface layers, *Coord. Chem. Rev.*, 1990, **97**, 237–248.

13 W. DeWilde G. Peeters and J. H. Lunsford, Synthesis and spectroscopic properties of tris(2,2′-bipyridine)ruthenium(II) in zeolite Y, *J. Phys. Chem.*, 1980, **84**, 2306–2310.

14 (*a*) M. Borja and P. K. Dutta, Storage of light energy by photoelectron transfer across a sensitized zeolite-solution interface, *Nature*, 1993, **362**, 43–45; (*b*) P. K. Dutta and W. Turbeville, Intrazeolitic photoinduced redox reactions between tris(2,2′-bipyridine)ruthenium(2+) and methylviologen, *J. Phys. Chem.*, 1992, **96**, 9410–9416; (*c*) P. K. Dutta and M. Borja, Separation of photogenerated redox species in zeolites via ion-exchange, *J. Chem. Soc., Chem. Commun.*, 1993, **20**, 1568–1569; (*d*) J. A. Incavo and P. K. Dutta, Zeolite host-guest interactions: optical spectroscopic properties of tris(bipyridine)ruthenium(II) in zeolite Y cages, *J. Phys. Chem.*, 1990, **94**, 3075–81; (*e*) K. Maruszewski and J. R. Kincaid, Dramatic Increase of ^{3}MLCT State Lifetimes of a Ruthenium(II) Polypyridine Complex upon Entrapment within Y-Zeolite Supercages, *Inorg. Chem.*, 1995, **34**, 2002–2006; (*f*) W. H. Quayle and J. H. Lunsford, Tris(2,2′-bipyridine)ruthenium(III) in zeolite Y: characterization and reduction on exposure to water, *Inorg. Chem.*, 1982, **21**, 97–103; (*g*) P. K. Dutta and J. A. Incavo, Photoelectron transfer from tris(2,2′-bipyridine)ruthenium(II) to methylviologen in zeolite cages: a resonance Raman spectroscopic study, *J. Phys. Chem.*, 1987, **91**, 4443–4446; (*h*) M. Ledney and P. K. Dutta, Oxidation of Water to Dioxygen by Intrazeolitic $Ru(bpy)_3^{3+}$, *J. Am. Chem. Soc.*, 1995, **117**, 7687–7691.

15 (*a*) Y. I. Kim and T. E. Mallouk, Dynamic electron-transfer quenching of the tris(2,2′-bipyridyl)ruthenium(II) MLCT excited state by intrazeolitic methylviologen ions, *J. Phys. Chem.*, 1992, **96**, 2879–2885; (*b*) J. S. Krueger, J. E. Mayer and T. E. Mallouk, Long-lived light-induced charge separation in a zeolite L-based molecular triad, *J. Am. Chem. Soc.*, 1988, **110**, 8232–8234; (*c*) Z. Li and T. E. Mallouk, Vectorial electron transport at ion-exchanged zeolite-Y-modified electrodes, *J. Phys. Chem.*, 1987, **91**, 643–648; (*d*) K. Maruszewski, D. P. Strommen, K. Handrich and J. R. Kincaid, Synthesis and spectroscopic properties of zeolite-entrapped bis-heteroleptic ruthenium(II) polypyridine complexes, *Inorg. Chem.*, 1991, **30**, 4579–4582.

16 C. Senaratne, J. Zhang, M. D. Baker, C. A. Bessel and D. R. Rolison, Zeolite-Modified Electrodes: Intra- versus Extra-zeolite Electron Transfer, *J. Phys. Chem.*, 1996, **100**, 5849.

17 W. S. Szulbinski and S. Malato, Photocatalytic wastewater treatment using the zeolite-Y entrapped ruthenium tris-2,2′-bipyridine complex, *Pol. J. Chem.*, 2001, **75**, 1543–1551.
18 S. K. Das and P. K. Dutta, Synthesis and characterization of a ruthenium oxide-zeolite Y catalyst for photochemical oxidation of water to dioxygen, *Microporous Mesoporous Mater.*, 1998, **22**, 475–483.
19 S. H. Bossmann, C. Turro, C. Schnabel, M. R. Pokhrel, L. M. Payawan Jr. and M. Wörner, $Ru(bpy)_3^{2+}/TiO_2$ Codoped Zeolites: Synthesis, Characterization, and the Role of TiO_2 in Electron Transfer Photocatalysis, *J. Phys. Chem. B.*, 2001, **105**, 5374–5382.
20 G. Cosa, M. N. Chretien, M. S. Galletero, V. Fornes, H. Garcia and J. C. Scaiano, Photocatalytic Activity of a Multicomponent System Assembled within Zeolites: Case of 2,4,6-Triphenylpyrylium or Ruthenium Tris(bipyridyl) Photosensitizers and Titanium Dioxide Relays within Zeolite Y, *J. Phys. Chem. B.*, 2002, **106**, 2460–2467.
21 For the definition of Advanced Oxidation Processes, see: O. Legrini, E. Oliveros and A. M. Braun, Photochemical processes for water treatment, *Chem. Rev.*, 1993, **93**, 671–698.
22 S. H. Bossmann, E. Oliveros, S. Göb, S. Siegwart, E. P. Dahlen, L. M. Payawan Jr, Matthias Straub, M. Wörner and A. M. Braun, New Evidence against Hydroxyl Radicals as Reactive Intermediates in the Thermal and Photochemically Enhanced Fenton Reactions, *J. Phys. Chem. A*, 1998, **102**, 5542–5550.
23 (*a*) S. L. Suib, Zeolitic and layered materials, *Chem. Rev.*, 1993, **93**, 908; (*b*) A. N. Fitch, H. Jobic and A. Renouprez, Localization of benzene in sodium-Y-zeolite by powder neutron diffraction, *J. Phys. Chem.*, 1986, **90**, 1311; (*c*) G. R. Eulenberger, D. P. Shoemaker and J. G. Keil, Crystal structures of hydrated and dehydrated synthetic zeolites with faujasite aluminosilicate frameworks. I. The dehydrated sodium, potassium, and silver forms, *J. Phys. Chem.*, 1967, **71**, 1812; (*d*) J. Klinowski, S. Ramdas, J. M. Thomas, C. A. Fyfe and J. S. Hartman, A reexamination of silicon, aluminum ordering in zeolites NaX and NaY, *J. Chem. Soc., Faraday Trans. 2*, 1982, **78**, 1025–1030.
24 A. Juris, F. Barigelletti, S. Campagna, V. Balzani, P. Belser and A. v. Zelewsky, Ruthenium(II) polypyridine complexes: photophysics, photochemistry, electrochemistry, and chemiluminescence, *Coord. Chem. Rev.*, 1988, **84**, 85–277.
25 (*a*) L. Kavan, B. O'Reagan, A. Kay and M. Grätzel, Preparation of titania (anatase) films on electrodes by anodic oxidative hydrolysis of titanium trichloride, *J. Electroanal. Chem.*, 1993, 291–307.
26 Based on photoacoustic measurements (L. Payawan, Jr, B. Schlageter, S. H. Bossmann and A. M. Braun, to be published) we estimated the thickness of the irradiated layer to be in the range from 100 to 10 nm, depending on the $[Ru(bpy)_3]^{2+}$ and TiO_2 content.
27 (*a*) W. T. Mo and J. Wei, Effective diffusivity in a partially blocked zeolite catalyst, *Chem. Eng. Sci.*, 1986, **41**, 703–710; (*b*) M. A. Garcia-Garibay, Z. Zhang and N. J. Turro, Diffusion and percolation of radical pairs in zeolite media. A product analysis study, *J. Am. Chem. Soc.*, 1991, **113**, 6212–6218; (*c*) S. S. Nivarthi, H. T. Davis and A. V. McCormick, Effectiveness of window blocking in zeolite NaY by strongly coadsorbed molecules, *Chem. Eng. Sci.*, 1995, **50**, 3217–3229; (*d*) D. Keffer, A. V. McCormick and H. T. Davis, Diffusion and Percolation on Zeolite Sorption Lattices, *J. Phys. Chem.*, 1996, **100**, 967–973.
28 K. Kalyanasundaram and M. Graetzel, Heterogeneous photocatalysis with semiconductor particulate systems. Springer Series in Chemical Physics, *Chem. Phys. Solid Surf. 5*, 1984, **35**, 111–139.
29 C. v. Sonntag and H.-P. Schuchmann, Elucidation of peroxyl radical reactions in aqueous solution with radiation chemistry technology, *Angew. Chem., Int. Ed. Engl.*, 1991, **30**, 1229–1253.
30 D. Barthomeuf, Zeolite acidity dependence on structure and chemical environment. Correlations with catalysis, *Mater. Chem. Phys.*, 1987, **17**, 49–71.
31 K. Sing, Physisorption of nitrogen by porous materials, *J. Porous Mater.*, 1995, **2**, 5–8.
32 K. Sing, The use of nitrogen adsorption for the characterization of porous materials, *Colloids Surf. A: Physicochem. Eng. Asp.*, 2001, **187–188**, 3–9.
33 S. H. Bossmann, S. Göb, T. Siegenthaler, A. M. Braun, K. T. Ranjit and I. Willner, An N,N′-dialkyl-4,4′-bipyridinium-modified titanium-dioxide photocatalyst for water remediation – observation and application of supramolecular effects in photocatalytic degradation of π-donor organic compounds, *Fresenius J. Anal. Chem*, 2001, **371**, 621–628.